Dispersion stabilizes metal-metal bonds in the 1,8-bis(silylamido)naphthalene ligand environment

Nicholas J. Roberts, Erin R. Johnson,* and Saurabh S. Chitnis*

Department of Chemistry, Dalhousie University, Halifax, Nova Scotia, Canada

E-mail: erin.johnson@dal.ca; saurabh.chitnis@dal.ca

Abstract

There is emerging consensus that stabilization of weak bonds using bulky substituents operates not only by steric shielding, but also by boosting the dispersive attraction across the bond. While many studies have explored this concept for hydrocarbon, arene, carbene, and phosphine ligands, it remains minimally explored for amide ligands. Bulky 1,8-bis(silylamido) naphthalenes were recently used to isolate the first example of Sb–Bi σ bonds, which was tentatively ascribed to an unexpectedly-high degree of inter-fragment dispersive stabilization. To understand this finding and study how the interplay between steric repulsion and dispersive attraction alters metal-metal bond strengths more generally, we have computationally examined Sb–Sb, Sb–Bi, and Bi–Bi σ bond enthalpies and energies in 21 compounds within the 1,8-bis(silylamido) naphthalenes ligand framework. The energies have been dissected into base electronic, dispersion, and ligand deformation contributions. The dispersion component has been further deconvoluted to identify the most significant pairwise functional group interactions driving dispersive stabilization. Steric clash has been considered by examining the extent of ligand deformation. The resulting insights will enable the rational evolution of these accessible and tunable ligands in the context of stabilizing weak bonds and may also be transferable to other amide ligands.

Introduction

Bulky substituents are often used to isolate fragile bonds. Such substituents keep reactive molecules away from the bond in question, and in the case of weak π bonds, also prevent dimerization or oligomerization (steric shielding, Figure 1a).[1,2] A second mechanism by which bulky groups preserve weak bonds is by increasing the overall bond dissociation enthalpies (BDEs) through peripheral dispersive attraction between the fragments (inter-fragment dispersion, Figure 1a).[3–5]

While these two factors stabilize bonds, high steric bulk can also increase Pauli repulsion (steric clash, Figure 1b), which lowers the BDE and makes a bond susceptible to fission.[6,7] In extreme cases, a putative bond may be so sterically hindered that its homolysis to give open-shell radicals becomes thermodynamically favourable. An application of this phenomenon is the successful isolation of persistent main group element radicals by using large flanking groups to prevent recombination of the radical fragments.[8–12]

Understanding this interplay between the stabilizing and destabilizing influences of large substituents is critical to ligand design and for providing a comprehensive view of bonding interactions within a ligand framework. While steric bulk and associated steric clashes are well-studied in organometallic chemistry, the importance of dispersion has only recently been recognized. For example, the dispersive stabilization from bulky aryl and alkyl substituents has been found to be key in enabling the isolation of very reactive organometallic compounds and predicting reactivity.[11,13–19] Similar studies have also been under-

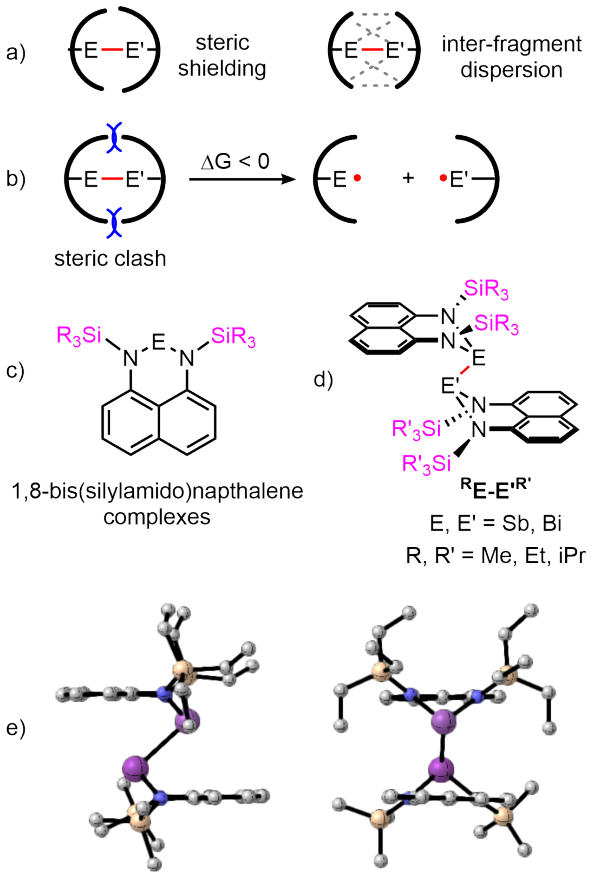

Figure 1: a) Steric shielding and inter-fragment dispersion as bond-stabilizing consequences of bulky groups. b) Steric clash as a bond-weakening consequence of bulky groups. c) A generic 1,8-bis(silylamido)naphthalene complex. d) Sb−Sb, Sb−Bi, and Bi−Bi σ bonded complexes studied here. e) Two views of the calculated structure of a representative example $^{\mathbf{Et}}\mathbf{Sb}-\mathbf{Bi}^{\mathbf{Me}}$ (hydrogen atoms omitted for clarity).

taken for carbene and phosphine ligands.[20–23] By comparison, few investigations have systematically and explicitly considered dispersive bond stabilization in complexes featuring bulky amide ligands, despite the prevalence of these ligands in coordination chemistry.[24–27]

Divalent 1,8-bis(silylamido) naphthalenes (Figure 1c) are popular ligands whose steric profiles can be easily tuned by an appropriate choice of inexpensive, diverse, and commercially-available chlorosilanes. This ligand framework also confers additional stability upon complexes due to the chelate effect. As a result, mono-metallic complexes featuring 1,8-bis(silylamido) naphthalenes ligands are known across the periodic table.[28–39]

We recently noted that these ligands also have the appropriate steric profile to stabilize very fragile bonds, and demonstrated this application by successfully isolating reactive antimony hydrides as well as the first examples of Sb–Bi σ bonds (Figure 1d,e).[40,41] In the latter case, our preliminary calculations suggested that the metal-metal bond energies for some derivatives were boosted by a remarkable 60% due to London dispersion. As a consequence, Sb–Bi σ bonds that rapidly decompose at 298 K when supported by small methyl groups[42] were stable for several days at 373 K when the 1,8-bis(silylamido) naphthalene ligand was used. Indeed, aryl and silyl groups have recently been recognized as being among the strongest dispersion-energy donors,[43] and the ligand system considered here features both. Clearly, steric bulk provides not only shielding of the metal-metal bond (as we had envisioned) but also has the potential to contribute a surprisingly large degree of inter-fragment dispersion to stabilize M-M bonds in this system.

These features suggest that 1,8-bis(silylamido) naphthalenes may be valuable scaffolds for accessing weak bonds more generally. However, to fully develop their potential in this context, it is necessary to understand the extent to which variation of steric bulk continually imparts stabilization before triggering significant Pauli repulsion, and which inter-fragment non-covalent interactions are the most significant determinants of bond stability.

We have therefore undertaken a detailed study of metal-metal BDEs in a systematically varied series of 1,8-bis(silylamido) naphthalene supported Sb–Sb, Sb–Bi, and Bi–Bi σ bonds. Most compounds in the series have already been crystallographically characterized, making it a bespoke family of compounds for such a study. We first calculate the overall metal-metal BDEs (which include thermal corrections) as a function of metals involved and the size of substituent used. The purely electronic bond energy, D_e (which excludes thermal corrections), was then calculated in each case and dissected into its base and dispersive contributions. The dispersion component is further decomposed into pairwise interactions between groups on each monometallic fragment to understand its functional group origins. Lastly, the strain accumulated within the fragments due to formation of the metal-metal bond has been quantified as a measure of steric clash.

The results are analyzed to reveal: i) the tipping point (in terms of silyl group bulk) between steric repulsion and dispersive attraction in this

system, ii) the most significant pairwise interactions that stabilize the metal-metal bond, and iii) the relative contributions of dispersive attraction and Pauli repulsion with varying silyl groups. Collectively, these insights provide guidance for further evolution of 1,8-bis(amido) naphthalene ligands and design principles that may also be transferable to other amide ligands used for isolating fragile bonds.

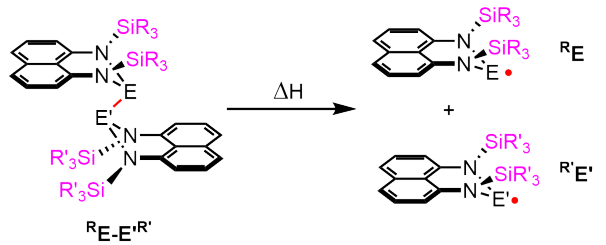

Figure 2: Reaction used for calculating BDEs in $^{\mathbf{R}}\mathbf{E}-\mathbf{E}'^{\mathbf{R}'}$.

Computational Methods

All calculations were performed with the Gaussian Suite[44] and the external postg program,[45,46] using the LC-ωPBE functional[47,48] and the exchange-hole dipole moment (XDM) dispersion correction.[45,49] Geometry optimizations and frequency calculations used 6-31G* for C, H, and Si, 6-31+G* for N, and the def2-SVP basis set and accompanying pseudopotential for Sb and Bi. All optimized structures showed zero negative frequencies. Single-point energy calculations were then performed on the optimized structures with the larger def2-TZVP basis set for all elements, which again uses a pseudopotential to replace the core electrons for Sb and Bi. The XDM parameters were set to 0.6889 and 1.9452 Å for the optimizations and 0.4741 and 2.3915 Å for the single-point energy evaluations.[50]

The BDEs correspond to the difference between the computed enthalpies of the radical products and metal-metal bonded reactants, as shown in Figure 2. The analogous electronic bond dissociation energies (D_e), without the zero-point energy and thermal enthalpy correction, were also computed to allow partitioning into base-functional and dispersion contributions. This partitioning is straightforward as the XDM dispersion energy is an additive, post-self-consistent correction to the energy from the base density functional.

$$E = E_{\text{base}} + E_{\text{disp}} \tag{1}$$

The XDM dispersion energy is expressed as a sum over all pairs of atoms i and j:

$$E_{\text{disp}} = -\sum_{i<j}\sum_{n=6,8,10}\frac{C_{n,ij}}{R_{ij}^{n}}f_n(R_{ij}), \tag{2}$$

where the $C_{n,ij}$'s are the dispersion coefficients for each atom pair and f_n is a damping function of the internuclear distance, R_{ij}. The pairwise interfragment dispersion contributions were determined using the critic2 program,[51] by limiting the summation in Eqn. 2 to the relevant atoms or functional groups.

Plots of the non-covalent interactions[52] were made using the nciplot[53] program. The fragment option was set to visualize only the interactions between the two halves of the complex.

Deformation energies for each fragment were estimated as the electronic energy difference between fully relaxed fragments and fragments frozen in the geometry they adopt in the metal-metal bonded compounds. The net deformation energy for each compound (given in Table 1) is the sum of the individual deformation energies of its constituent fragments.

Results and discussion

The metal-metal bond lengths for compounds $^{\mathbf{R}}\mathbf{E}-\mathbf{E}'^{\mathbf{R}'}$, as well as their BDEs and D_e values (calculated as per Figure 2) are given in Table 1. The D_e values are represented graphically in Figure 3, where they are further partitioned into their base electronic and dispersion components.

The intermetallic bond lengths span an approximately 0.2 Å range, with Sb−Sb, Sb−Bi, and Bi−Bi bonded derivatives showing mean values of 2.846, 2.919, and 2.994 Å, respectively. These numbers vary in line with the covalent radii for the metals involved (1.40 Å for Sb and 1.50 Å for Bi),[54] and are marginally shorter than the experimentally-known mean values of 2.903 Å, 2.980 Å, and 3.069 Å.[40,41] Within each type of bond, there is a small increase in bond length with increasing steric bulk. For example, the Sb−Sb bond increases by 0.07 Å going from $^{\mathbf{Me}}\mathbf{Sb}-\mathbf{Sb}^{\mathbf{Me}}$ to $^{\mathbf{iPr}}\mathbf{Sb}-\mathbf{Sb}^{\mathbf{iPr}}$. Despite this increase, there is no overlap between the calculated bond length ranges of the three types

of intermetallic bonds considered. All BDEs lie in the 47–55 kcal/mol range, in full agreement with the reported high thermal stability of the known derivatives.[40,41]

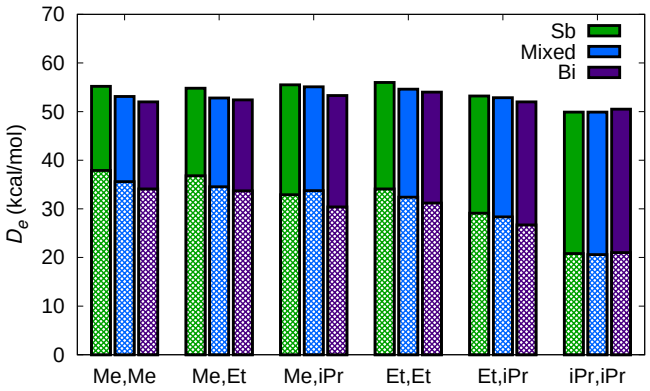

Figure 3: Dissociation energies (D_e) for the various $^{\mathbf{R}}\mathbf{E}-\mathbf{E}'^{\mathbf{R}'}$ complexes, showing their decomposition into base electronic (cross-hatched) and dispersion (solid) contributions. For the mixed-metal cases with differing alkyl substitution, the average of the results for the two possible complexes is shown.

Variations in D_e values

As a function of silyl steric bulk

As shown in Figure 3, the electronic bond energies (D_e's) increase as the steric bulk of the silyl groups is increased up to a point defined by the presence of two $SiEt_3$ groups on both sides of the metal-metal bond. The D_e's then decrease as iPr groups are added, with the lowest value being observed in the doubly-iPr substituted compounds. If only the base electronic component of the D_e is considered (cross-hatched bars in Figure 3), the values monotonically decrease with increased steric bulk, with a sharp drop in the D_e for the case with full iPr substitution. Thus consideration of the dispersion component (solid bars in Figure 3) is clearly important in understanding the overall bond strength trends.

Both the absolute value and percent contribution of dispersion to the overall D_e increases with size of the silyl substituent. In the case of fully iPr substituted compounds, dispersion contributes approximately 30 kcal/mol to the D_e, representing ∼60% of its calculated value. However, steric repulsion from these groups is also considerable (*vide infra*), leading to the aforementioned maximum in D_e values for full $SiEt_3$ substitution. Further increasing the substituent size still increases the dispersive stabilization, but insufficiently so to offset the accompanying increase in steric repulsion, resulting in overall lowering of D_e for the iPr-substituted compounds.

As a function of metal involved

Figure 3 shows that for five out of six substitution patterns tested, the lighter Sb−Sb bond was found to be stronger than the corresponding Sb−Bi or Bi−Bi bond, in line with the generally observed trend that σ bond strengths decrease descending a periodic group. Only in the case of full substitution with $Si(iPr)_3$ groups does the heavier bond show a higher D_e. Interestingly, the absolute value of dispersion does not vary substantially as a function of the identity of the metal involved. For example, the dispersion stabilization in $^{\mathbf{Me}}\mathbf{Sb}-\mathbf{Sb}^{\mathbf{Me}}$, $^{\mathbf{Me}}\mathbf{Sb}-\mathbf{Bi}^{\mathbf{Me}}$, and $^{\mathbf{Me}}\mathbf{Bi}-\mathbf{Bi}^{\mathbf{Me}}$ is approximately 17.5 kcal/mol, representing approximately 30–35% of the net D_e in each case. Thus, a simple argument invoking the relative polarizabilities of the metals does not adequately explain the observed D_e span.

Functional group contributions to dispersion

As the preceding discussion shows, inclusion of dispersion is essential for understanding D_e trends within the 1,8-bis(silylamido) naphthalene ligand framework, and this dispersive stabilization originates primarily from the ligand rather than the metal. However, the data in Figure 3 and Table 1 do not reveal the precise interactions that are the strongest contributors to the net dispersion stabilization. In contrast, the base-functional energy changes upon bonding are readily understood as being primarily due to the stabilization originating from the orbital and electrostatic changes accompanying metal-metal σ bond formation.

For a bird's eye view of where dispersive interactions may be found in the compounds considered here, we began with an analysis of the non-covalent interactions within $^{\mathbf{Et}}\mathbf{Sb}-\mathbf{Sb}^{\mathbf{Et}}$. Such interactions can be conveniently visualized using an NCIplot, which highlights regions of low reduced density gradient and low electron density that are indicative of non-covalent interactions.[53] Figure 4 shows two views of $^{\mathbf{Et}}\mathbf{Sb}-\mathbf{Sb}^{\mathbf{Et}}$ along with isosurfaces ($s = 0.5$) to highlight the non-covalent interactions between the two halves of the molecule. The

Table 1: Calculated metal-metal bond lengths (R in Å), BDEs, and D_e's, along with the base functional and dispersion contributions to the D_e's, and the deformation energies. All energy values are given in kcal/mol. Values in parentheses show the relative contribution made by the base-functional or dispersion term to the total D_e.

Entry	**Compound**	**R**	**BDE**	**D_e**	**Base**	**Dispersion**	**Deformation**
	Bi−Bi						
1	^{Me}Bi−Bi^{Me}	2.977	50.7	52.0	34.1 (66%)	17.9 (34%)	2.1
2	^{Me}Bi−Bi^{Et}	2.984	51.2	52.5	33.7 (64%)	18.7 (36%)	2.4
3	^{Me}Bi−Bi^{iPr}	2.981	51.9	53.3	30.4 (57%)	22.9 (43%)	4.3
4	^{Et}Bi−Bi^{Et}	2.991	52.3	53.9	31.2 (57%)	22.8 (43%)	2.3
5	^{Et}Bi−Bi^{iPr}	3.002	50.2	52.0	26.7 (51%)	25.3 (49%)	6.2
6	^{iPr}Bi−Bi^{iPr}	3.031	48.6	50.5	21.0 (42%)	29.5 (58%)	6.8
	Sb−Sb						
7	^{Me}Sb−Sb^{Me}	2.824	53.8	55.2	37.9 (69%)	17.3 (31%)	1.2
8	^{Me}Sb−Sb^{Et}	2.834	53.3	54.8	36.8 (67%)	18.0 (33%)	1.7
9	^{Me}Sb−Sb^{iPr}	2.841	53.8	55.5	32.9 (59%)	22.6 (41%)	3.8
10	^{Et}Sb−Sb^{Et}	2.834	54.4	56.0	34.1 (61%)	21.9 (39%)	3.2
11	^{Et}Sb−Sb^{iPr}	2.851	51.7	53.2	29.1 (55%)	24.1 (45%)	6.4
12	^{iPr}Sb−Sb^{iPr}	2.892	47.6	49.9	20.8 (42%)	29.1 (58%)	7.7
	Sb−Bi						
13	^{Me}Sb−Bi^{Me}	2.903	51.9	53.2	35.6 (67%)	17.5 (33%)	1.7
14	^{Me}Sb−Bi^{Et}	2.910	52.1	53.5	35.1 (66%)	18.4 (34%)	1.8
15	^{Et}Sb−Bi^{Me}	2.905	50.7	52.1	34.0 (65%)	18.1 (35%)	2.8
16	^{Me}Sb−Bi^{iPr}	2.906	53.4	55.0	33.4 (61%)	21.6 (39%)	2.3
17	^{iPr}Sb−Bi^{Me}	2.908	53.6	55.2	34.1 (62%)	21.1 (38%)	1.6
18	^{Et}Sb−Bi^{Et}	2.911	53.0	54.5	32.4 (59%)	22.2 (41%)	3.3
19	^{Et}Sb−Bi^{iPr}	2.931	51.2	52.8	27.9 (53%)	24.9 (47%)	5.7
20	^{iPr}Sb−Bi^{Et}	2.932	51.1	53.0	28.8 (54%)	24.1 (46%)	5.3
21	^{iPr}Sb−Bi^{iPr}	2.964	47.7	49.8	20.6 (41%)	29.3 (59%)	7.1

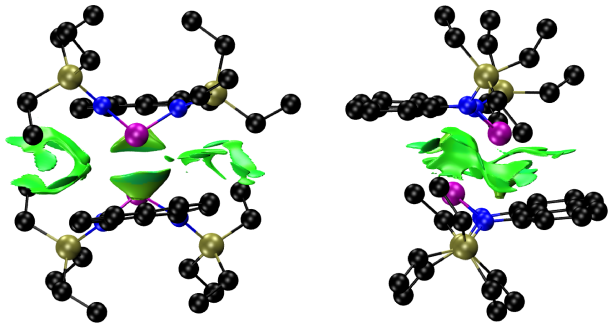

Figure 4: Isosurfaces showing non-covalent interactions between the two $\mathbf{Sb^{Et}}$ moeities in $\mathbf{^{Et}SbSb^{Et}}$ from two perspectives.

green colouring can be interpreted as representing non-bonding, dispersion interactions. From this plot, stabilizing interactions that buttress the intermetallic bond can be clearly observed between i) the silyl substituents (SiR_3-SiR'_3), ii) the metal centres and the naphthyl groups (M-Nap′, M′-Nap), and iii) the silyl groups and the napthyl groups (Nap′-SiR_3, Nap-SiR'_3). Table 2 quantifies these pair-wise dispersive interactions along with dispersive interactions between the metal atoms (M-M′), the naphthyl groups (Nap-Nap′), and the metal atoms and the silyl groups (M-SiR'_3, M′-SiR_3). The results are also shown graphically in Figure 5.

One of the two most significant contributors to the dispersion energy is the interactions between metal atoms and the naphthalene rings (M-Nap′ and M′-Nap). Such interactions are experimentally well-known for antimony and bismuth compounds, which form strongly bound solvent adducts with aromatic hydrocarbons.[55] Summing to ca. 6-8 kcal/mol in all derivatives studied here, this interaction represents one-third of the total dispersive stabilization, and its large magnitude suggests the naphthalenediamine framework may be intrinsically suited for boosting bond energies, particularly when polarizable heavy elements are involved.

Dispersion between the silyl groups and naphthyl rings (Nap′-SiR_3 and Nap-SiR'_3) is the second major contributor. Here the values show more variation (5-10 kcal/mol range), with greater stabilization observed for larger silyl groups. In all cases except the R=Me and R′=Me,Et substituted derivatives, the silyl-naphthyl interaction is stronger than even the metal-naphthyl dispersive interactions.

As anticipated, the largest variation is observed for dispersion between the silyl groups (SiR_3-SiR'_3, 0-5 kcal/mol range). The values increase substan-

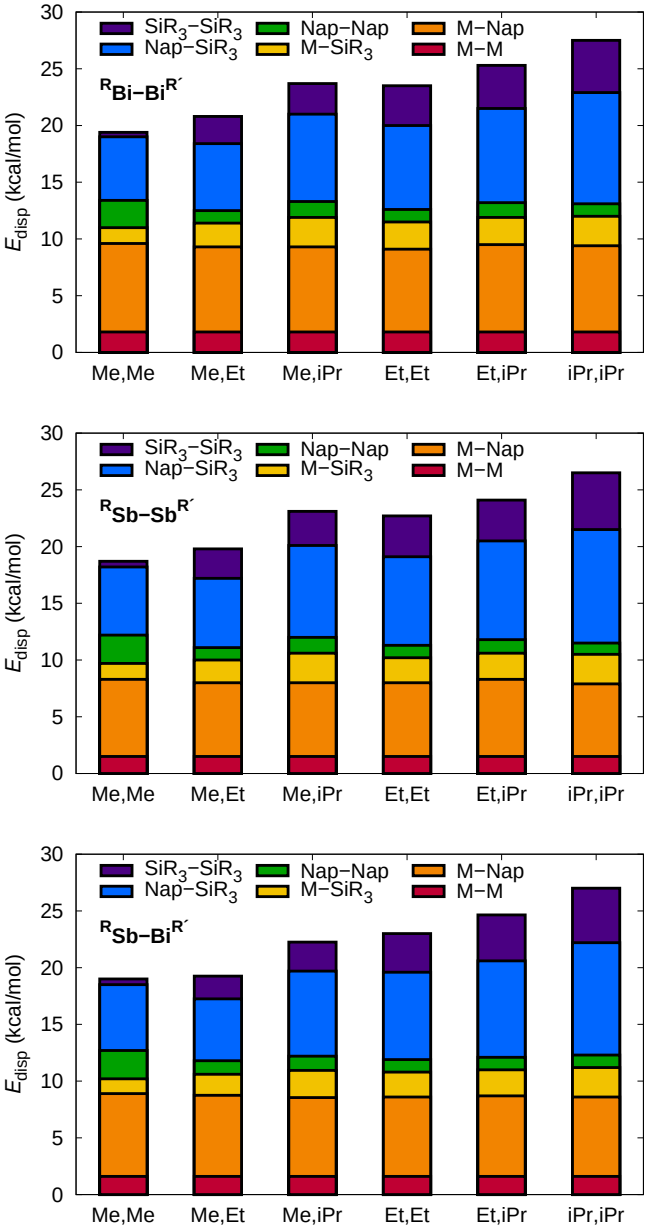

Figure 5: Stack plot showing the pairwise dispersive interactions between selected functional groups in derivatives of $\mathbf{^{R}BiBi^{R'}}$ (top),$\mathbf{^{R}SbSb^{R'}}$ (middle), and $\mathbf{^{R}SbBi^{R'}}$ (bottom). For the mixed-metal cases with differing alkyl substitution, the average of the results for the two possible complexes is shown.

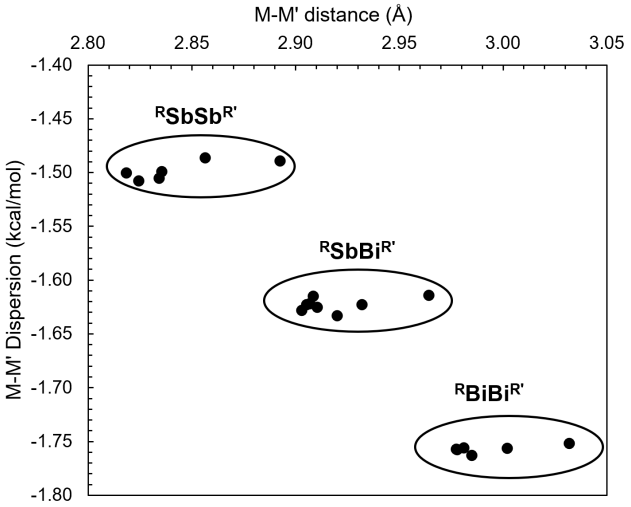

Figure 6: Variation in the M–M′ dispersion energy with M–M′ bond distance.

tially with the size of the group – minimal contributions are observed for the $SiMe_3$ group but significant ones for $SiEt_3$ and $Si(iPr)_3$ – in line with the small but additive nature of van der Waals attraction.

Interestingly, despite being well-separated, the dispersion between the naphthyl rings is nontrivial (1-3 kcal/mol range). The values for the $SiMe_3$ substituted compounds are consistently the highest across all three bond types, and they decrease as the bulk of the silyl substituent increases. This trend is interpreted as being a consequence of the elongation of the metal-metal bond upon installation of a bulky silyl group that, in turn, also increases the distance between the aromatic groups, thereby reducing dispersion.

The dispersive interaction between the metal atoms can be expected to vary strongly with either the bond length or the polarizability of the elements involved. Figure 6 shows that within a given bond family, there is minimal variation in dispersive stabilization, even when the bond distance varies substantially. This is expected since the dispersion energy of Eqn 2 is heavily damped at small internuclear distances, as occur for covalent bonds. On the other hand, introducing a heavy element abruptly increases the dispersive stabilization. Even for boundary cases where the bond length ranges between bonding families almost overlap, there is still a significant change in dispersion. Thus, it is the element polarizability rather than the bond distance, that primarily determines the extent of stabilization between the metal atoms within this ligand framework. Note, however, that the magnitude of the contributions is still rather small, compared to dispersion contributions from other parts of the molecules.

Steric Clashes

We also considered the contribution of steric repulsion to the D_e values by summing the energy cost incurred for structurally deforming the two $^{\mathbf{R}}\mathbf{E}$ fragments from their equilibrium geometries to the geometry adopted in the respective metal-metal bonded compound (Table 1). A representative example of the ligand deformation observed is shown in Figure 7, where one of the silyl arms in $^{\mathbf{iPr}}\mathbf{Bi}$ is twisted to point above the plane of the naphthalene ring to accommodate a second equivalent in the full molecule, $^{\mathbf{iPr}}\mathbf{BiBi}^{\mathbf{iPr}}$.

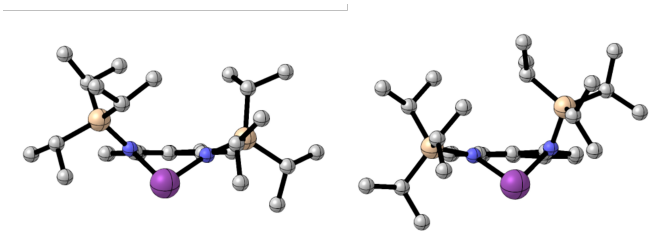

Figure 7: Views of the $^{\mathbf{iPr}}\mathbf{Bi}$ radical in its equilibrium geometry (left) and in the geometry it adopts in $^{\mathbf{iPr}}\mathbf{BiBi}^{\mathbf{iPr}}$ (right).

As listed in Table 1, the deformation energy values lie in the 1–8 kcal/mol range, which makes them as significant as the most important dispersive interactions in some cases, but an order of magnitude smaller than the total dispersive stabilization. Thus, dispersive attraction clearly dominates over steric clash within this ligand framework, even when very bulky $Si(iPr)_3$ groups are employed.

Within a given bonding series, the deformation energy increases with the size of the silyl substituent. For example, derivatives of $^{\mathbf{Me}}\mathbf{MM'}^{\mathbf{Me}}$ experience a penalty of ca. 1–2 kcal/mol but derivatives of $^{\mathbf{iPr}}\mathbf{MM'}^{\mathbf{iPr}}$ experience a penalty of 7–8 kcal/mol. Such an increase with the size of the silyl substituent is expected because larger groups experience greater Pauli repulsion, which scales with number of electrons involved, and more bond angles and lengths must be distorted in the resulting deviation away from their equilibrium geometries.

Table 2: Contributions to the bond dissociation energies (D_e in kcal/mol) from the various pairwise interfragment dispersion interactions. "Nap" indicates the atoms within the naphthalene rings, including the N atoms. For cases with differing alkyl substituents, the result for the more bulky group is shown first, otherwise the largest contribution to the D_e is shown first.

Entry	Compound	Total	E−E′	E−Nap′	E′−Nap	E−SiR$_3$′	E′−SiR$_3$	Nap-Nap′	Nap-SiR′$_3$	Nap′-SiR$_3$	SiR$_3$−SiR′$_3$
	Bi−Bi										
1	^{Me}Bi−Bi^{Me}	19.5	1.8	3.9	3.9	0.7	0.7	2.4	2.8	2.8	0.4
2	^{Me}Bi−Bi^{Et}	20.6	1.8	4.0	3.5	1.3	0.8	1.1	3.6	2.3	2.4
3	^{Me}Bi−Bi^{iPr}	23.8	1.8	3.9	3.6	1.9	0.7	1.4	5.2	2.5	2.7
4	^{Et}Bi−Bi^{Et}	23.1	1.8	3.7	3.6	1.2	1.2	1.1	3.8	3.5	3.5
5	^{Et}Bi−Bi^{iPr}	25.3	1.8	4.0	3.7	1.6	0.8	1.3	5.0	3.3	3.8
6	^{iPr}Bi−Bi^{iPr}	27.4	1.8	3.9	3.7	1.3	1.3	1.1	5.0	4.8	4.6
	Sb−Sb										
7	^{Me}Sb−Sb^{Me}	18.7	1.5	3.4	3.4	0.7	0.7	2.5	3.0	3.0	0.5
8	^{Me}Sb−Sb^{Et}	19.8	1.5	3.5	3.0	1.2	0.8	1.1	3.6	2.5	2.6
9	^{Me}Sb−Sb^{iPr}	23.0	1.5	3.4	3.1	1.9	0.7	1.4	5.4	2.7	3.0
10	^{Et}Sb−Sb^{Et}	22.7	1.5	3.5	3.0	1.1	1.1	1.1	4.2	3.6	3.6
11	^{Et}Sb−Sb^{iPr}	24.2	1.5	3.7	3.1	1.4	0.9	1.2	4.8	3.9	3.6
12	^{iPr}Sb−Sb^{iPr}	26.6	1.5	3.3	3.1	1.3	1.3	1.0	5.0	5.0	5.0
	Sb−Bi										
13	^{Me}Sb−Bi^{Me}	19.0	1.6	3.9	3.4	0.7	0.6	2.5	3.0	2.8	0.5
14	^{Me}Sb−Bi^{Et}	19.2	1.6	3.5	3.5	1.2	0.6	1.1	3.5	2.1	2.2
15	^{Et}Sb−Bi^{Me}	19.3	1.6	3.9	3.4	1.3	0.6	1.3	3.8	1.5	1.8
16	^{Me}Sb−Bi^{iPr}	22.5	1.6	3.6	3.3	1.7	0.7	1.3	5.3	2.3	2.7
17	^{iPr}Sb−Bi^{Me}	22.0	1.6	3.9	3.1	1.8	0.6	1.2	5.3	2.1	2.4
18	^{Et}Sb−Bi^{Et}	23.1	1.6	3.5	3.5	1.1	1.1	1.1	4.2	3.5	3.4
19	^{Et}Sb−Bi^{iPr}	24.9	1.6	3.7	3.4	1.3	1.0	1.1	5.2	3.7	3.9
20	^{iPr}Sb−Bi^{Et}	24.4	1.6	3.9	3.2	1.5	0.8	1.1	5.1	3.0	4.2
21	^{iPr}Sb−Bi^{iPr}	26.9	1.6	3.7	3.3	1.4	1.2	1.1	5.0	4.9	4.8

Conclusions

We have examined trends in BDE and D_e values across a systematically varied family of Sb−Sb, Sb−Bi, and Bi−Bi compounds within the 1,8-disilylnaphthalene diamine ligand framework. The calculated BDEs, which are in the 47–54 kcal/mol range, bear out the experimentally-observed high metal-metal bond strength in these compounds. Analysis of the electronic bond energies (D_e's) shows that dispersion plays a key role in stabilizing the bond, and provides 17-29 kcal/mol of the total stabilization. Quantitative comparison of the dispersive stabilization with steric repulsion – as codified by the ligand deformation energies – clearly identifies dispersion as being the dominant interaction. Even for the fully iPr substituted case, the dispersion stabilization is higher than the deformation energy by a factor of roughly 4 across this family of compounds.

Deconvolution of the dispersive interactions into its pair-wise functional group contribution identifies metal-naphthyl and silyl-naphthyl interactions as being the two biggest contributors, with the silyl-silyl interaction being a close third. Dispersion between the metal centers is driven primarily by their polarizability rather than the metal-metal bond distance, but makes a rather small contribution, despite the high polarizability of these electropositive 5th and 6th row metals.

Silyl-groups are involved in two out of the three most significant dispersion interactions, leading to well-defined trends in the overall BDEs as a function of silyl group variation. Since these groups are also experimentally very straightforward to modify (being installed from commercially available chlorosilanes), they offer a convenient means of tuning the metal-metal BDEs over a 7–8 kcal/mol range, representing a significant fraction of the total bonding.

These results highlight the ability of 1,8-bis(silylamido) naphthalene ligands, when decorated with judiciously chosen groups, to stabilize fragile bonds in a highly tunable fashion. Understanding the origins and relative magnitudes of the BDEs involved now also provides a rational basis for evolving functional reactivity where either retention or fission of the metal-metal bond may be desirable.

Acknowledgement We thank the Natural Sciences & Engineering Research Council of Canada and Dalhousie University for funding, and Compute Canada for the use of high performance computing infrastructure.

Supporting Information Available

Cartesian coordinates of optimized structures.

References

(1) Some highlights from the development and use of bulky monodentate ligands. *J. Organomet. Chem.* **2004**, *689*, 3904–3919.

(2) Kays, D. L. Extremely bulky amide ligands in main group chemistry. *Chem. Soc. Rev.* **2016**, *45*, 1004–1018.

(3) Liptrot, D. J.; Power, P. P. London dispersion forces in sterically crowded inorganic and organometallic molecules. *Nat. Rev. Chem.* **2017**, *1*, 0004.

(4) Power, P. P. An Update on Multiple Bonding between Heavier Main Group Elements: The Importance of Pauli Repulsion, Charge-Shift Character, and London Dispersion Force Effects. *Organometallics* **2020**, *39*, 4127–4138.

(5) Wagner, J. P.; Schreiner, P. R. London Dispersion in Molecular Chemistry—Reconsidering Steric Effects. *Angew. Chem. Int. Ed. 54*, 12274–12296.

(6) Rösel, S.; Becker, J.; Allen, W. D.; Schreiner, P. R. Probing the Delicate Balance between Pauli Repulsion and London Dispersion with Triphenylmethyl Derivatives. *J. Am. Chem. Soc.* **2018**, *140*, 14421–14432.

(7) Wiberg, N.; Amelunxen, K.; Blank, T.; Nöth, H.; Knizek, J. Tetrasupersilyldialuminum $[(t{-}Bu)_3Si]_2Al{-}Al[Si(t{-}Bu)_3]_2$: The Dialane(4) with the Longest Al–Al Bond to Date,. *Organometallics* **1998**, *17*, 5431–5433.

(8) Power, P. P. Persistent and Stable Radicals of the Heavier Main Group Elements and Related Species. *Chem. Rev.* **2003**, *103*, 789–810.

(9) Pan, X.; Chen, X.; Li, T.; Li, Y.; Wang, X. Isolation and X-ray Crystal Structures of Triarylphosphine Radical Cations. *J. Am. Chem. Soc.* **2013**, *135*, 3414–3417.

(10) Helling, C.; Schulz, S. Long-Lived Radicals of the Heavier Group 15 Elements Arsenic, Antimony, and Bismuth. *Eur. J. Inorg. Chem.* **2020**, *34*, 3209–3221.

(11) Guo, J.-D.; Nagase, S.; Power, P. P. Dispersion Force Effects on the Dissociation of "Jack-in-the-Box" Diphosphanes and Diarsanes. *Organometallics* **2015**, *34*, 2028–2033.

(12) Tan, G.; Wang, X. Isolable Radical Ions of Main-Group Elements: Structures, Bonding and Properties. *Chin. J. Chem.* **2018**, *36*, 573–586.

(13) Mears, K. L.; Power, P. P. Beyond Steric Crowding: Dispersion Energy Donor Effects in Large Hydrocarbon Ligands. *Acc. Chem. Res.* **2022**, *55*, 1337–1348.

(14) Grimme, S.; Djukic, J.-P. Cation-Cation "Attraction": When London Dispersion Attraction Wins over Coulomb Repulsion. *Inorg. Chem.* **2011**, *50*, 2619–2628.

(15) Solel, E.; Ruth, M.; Schreiner, P. R. London Dispersion Helps Refine Steric A-Values: Dispersion Energy Donor Scales. *J. Am. Chem. Soc.* **2021**, *143*, 20837–20848.

(16) Bursch, M.; Caldeweyher, E.; Hansen, A.; Neugebauer, H.; Ehlert, S.; Grimme, S. Understanding and Quantifying London Dispersion Effects in Organometallic Complexes. *Acc. Chem. Res.* **2019**, *52*, 258–266.

(17) Arp, H.; Baumgartner, J.; Marschner, C.; Zark, P.; Müller, T. Dispersion Energy Enforced Dimerization of a Cyclic Disilylated Plumbylene. *J. Am. Chem. Soc.* **2012**, *134*, 6409–6415.

(18) Guo, J.-D.; Liptrot, D. J.; Nagase, S.; Power, P. P. The multiple bonding in heavier group 14 element alkene analogues is stabilized mainly by dispersion force effects. *Chem. Sci.* **2015**, *6*, 6235–6244.

(19) Queen, J. D.; Bursch, M.; Seibert, J.; Maurer, L. R.; Ellis, B. D.; Fettinger, J. C.; Grimme, S.; Power, P. P. Isolation and Computational Studies of a Series of Terphenyl

Substituted Diplumbynes with Ligand Dependent Lead–Lead Multiple-Bonding Character. *J. Am. Chem. Soc.* **2019**, *141*, 14370–14383.

(20) Wagner, J. P.; Schreiner, P. R. London Dispersion Decisively Contributes to the Thermodynamic Stability of Bulky NHC-Coordinated Main Group Compounds. *J. Chem. Theory Comput.* **2016**, *12*, 231–237.

(21) Xi, Y.; Su, B.; Qi, X.; Pedram, S.; Liu, P.; Hartwig, J. F. Application of Trimethylgermanyl-Substituted Bisphosphine Ligands with Enhanced Dispersion Interactions to Copper-Catalyzed Hydroboration of Disubstituted Alkenes. *J. Am. Chem. Soc.* **2020**, *142*, 18213–18222.

(22) Lu, G.; Liu, R. Y.; Yang, Y.; Fang, C.; Lambrecht, D. S.; Buchwald, S. L.; Liu, P. Ligand–Substrate Dispersion Facilitates the Copper-Catalyzed Hydroamination of Unactivated Olefins. *J. Am. Chem. Soc.* **2017**, *139*, 16548–16555.

(23) Burgos, J. C.; Mejía, S. M.; Metha, G. F. Effect of Charge and Phosphine Ligands on the Electronic Structure of the Au8 Cluster. *ACS Omega* **2019**, *4*, 9169–9180.

(24) Liu, J.; Bollmeyer, M. M.; Kim, Y.; Xiao, D.; MacMillan, S. N.; Chen, Q.; Leng, X.; Kim, S. H.; Zhao, L.; Lancaster, K. M.; Deng, L. An Isolable Mononuclear Palladium(I) Amido Complex. *J. Am. Chem. Soc.* **2021**, *143*, 10751–10759.

(25) Lin, C.-Y.; Guo, J.-D.; Fettinger, J. C.; Nagase, S.; Grandjean, F.; Long, G. J.; Chilton, N. F.; Power, P. P. Dispersion Force Stabilized Two-Coordinate Transition Metal–Amido Complexes of the -N($SiMe_3$)Dipp (Dipp = C_6H_3−2,6−iPr_2) Ligand: Structural, Spectroscopic, Magnetic, and Computational Studies. *Inorg. Chem.* **2013**, *52*, 13584–13593.

(26) Song, L.; Schoening, J.; Wölper, C.; Schulz, S.; Schreiner, P. R. Role of London Dispersion Interactions in Ga-Substituted Dipnictenes. *Organometallics* **2019**, *38*, 1640–1647.

(27) Pandey, K. K.; Patidar, P. Dispersion interactions with density functional theory: Bonding description of V–NS bond in vanadium–thionitrosyl complex [(nacnac)(OAr)V(NS)]. *Computational and Theoretical Chemistry* **2014**, *1028*, 1–6.

(28) Avent, A. G.; Drost, C.; Gehrhus, B.; Hitchcock, P. B.; Lappert, M. F. Synthetic and structural studies on the cyclic bis(amino)stannylenes Sn[$(NR)_2C_{10}H_6$−1,8] and their reactions with $SnCl_2$ or Si[$(NCH_2But)_2C_6H_4$−1,2] (R = $SiMe_3$ or CH_2tBu). *Z. Anorg. Allg. Chem.* **2004**, *630*, 2090–2096.

(29) Bradley, M. A.; Birchall, C.; Blake, A. J.; Lewis, W.; Moxey, G. J.; Kays, D. L. 1,8-Bis(silylamido)naphthalene complexes of magnesium and zinc synthesised through alkane elimination reactions. *Dalton Trans.* **2017**, *46*, 4101–4110.

(30) Galka, C. H.; Troesch, D. J. M.; Ruedenauer, I.; Gade, L. H.; Scowen, I.; McPartlin, M. Synthesis and Structural Characterization of Metalated 1,8-Bis(silylamino)naphthalene Derivatives. *Inorg. Chem.* **2000**, *39*, 4615–4620.

(31) Hellmann, K.; Galka, C. H.; Rudenauer, I.; Gade, L. H.; Scowen, I. J.; McPartlin, M. Metal-ligand versus metal-metal redox chemistry: thallium(I)-induced synthesis of 4,9-diaminoperylenequinone-3,10-diimine derivatives. *Angew. Chem., Int. Ed.* **1998**, *37*, 1948–1952.

(32) Jimenez-Perez, V. M.; Munoz-Flores, B. M.; Roesky, H. W.; Schulz, T.; Pal, A.; Beck, T.; Yang, Z.; Stalke, D.; Santillan, R.; Witt, M. Monomeric boron and Tin(II) heterocyclic derivatives of 1,8-diaminonaphthalenes: synthesis, characterization and X-ray structures. *Eur. J. Inorg. Chem.* **2008**, 2238–2243.

(33) Koner, A.; Sergeieva, T.; Morgenstern, B.; Andrada, D. M. A Cyclic Iminoborane-NHC Adduct: Synthesis, Reactivity, and Bonding Analysis. *Inorg. Chem.* **2021**, *60*, 14202–14211.

(34) Lee, C. H.; La, Y.-H.; Park, S. J.; Park, J. W. Preparation of N,N'-Disilylated

1,8-Diaminonaphthalene Chelates and Their Group 4 Metal Complexes for Ethylene Polymerization. *Organometallics* **1998**, *17*, 3648–3655.

(35) Lyubov, D. M.; Fukin, G. K.; Trifonov, A. A. New yttrium complexes with the 1,8-bis(trimethylsilylamido)naphthalene ligand. The molecular structures of complexes $[1,8{-}C_{10}H_6(NSiMe_3)_2YCl(DME)]_2$ $(\mu{-}Cl)[Li(DME)_3]$ and $\{[1,8{-}C_{10}H_6(NSiMe_3)_2]YN(SiMe_3)_2$ $(\mu{-}Cl)\}_2$ $\{Li(DME)_3\}_2$. *Russ. Chem. Bull.* **2010**, *58*, 522–527.

(36) Nekoueishahraki, B.; Sarish, S. P.; Roesky, H. W.; Stern, D.; Schulzke, C.; Stalke, D. Addition of Dimethylaminobismuth to Aldehydes, Ketones, Alkenes, and Alkynes. *Angew. Chem., Int. Ed.* **2009**, *48*, 4517.

(37) Nomura, K.; Naga, N.; Takaoki, K.; Imai, A. Synthesis of titanium(IV) complexes that contain the Bis(silylamide) ligand of the type $[1,8{-}C_{10}H_6(NR)_2]^{2-}$, and alkene polymerization catalyzed by $[1,8{-}C_{10}H_6(NR)_2]TiCl_2$-cocatalyst system. *J. Mol. Catal. A: Chem.* **1998**, *130*, L209.

(38) Sarish, S. P.; Nekoueishahraki, B.; Jana, A.; Roesky, H. W.; Schulz, T.; Stalke, D. A New Entry into Aluminum Chemistry: [L1AlMe]·THF, a Versatile Building Block for Bimetallic and Polymetallic Complexes. *Chem. - Eur. J.* **2011**, *17*, 890.

(39) Takaoki, K.; Nomura, K.; Naga, N.; Imai, A. Synthesis of titanium complexes containing bis(silylamide) ligand for olefin polymerization. *Stud. Surf. Sci. Catal.* **1999**, *121*, 469–472.

(40) Marczenko, K. M.; Chitnis, S. S. Bismuthanylstibanes. *Chem. Commun.* **2020**, *56*, 8015–8018.

(41) Marczenko, K. M.; Zurakowski, J. A.; Bamford, K. L.; MacMillan, J. W. M.; Chitnis, S. S. Hydrostibination. *Angew. Chem. Int. Ed.* **2019**, *58*, 18096–18101.

(42) Ashe, A. J.; Ludwig, E. G. The exchange reaction of tetramethyl-diphosphine, -diarsine, -distibine and -dibismuthine. *J. Organomet. Chem.* **1986**, *303*, 197–204.

(43) Pollice, R.; Chen, P. A Universal Quantitative Descriptor of the Dispersion Interaction Potential. *Angew. Chem. Int. Ed.* **2019**, *58*, 9758–9769.

(44) Frisch, M. J. et al. Gaussian 09 Revision E.01. Gaussian Inc. Wallingford CT 2009.

(45) Otero-de-la-Roza, A.; Johnson, E. R. Non-Covalent Interactions and Thermochemistry using XDM-Corrected Hybrid and Range-Separated Hybrid Density Functionals. *J. Chem. Phys.* **2013**, *138*, 204109.

(46) The postg code is available from http://schooner.chem.dal.ca/wiki/postg.

(47) Vydrov, O. A.; Scuseria, G. E. Assessment of a long-range corrected hybrid functional. *J. Chem. Phys.* **2006**, *125*, 234109.

(48) Vydrov, O. A.; Heyd, J.; Krukau, A. V.; Scuseria, G. E. Importance of short-range versus long-range Hartree-Fock exchange for the performance of hybrid density functionals. *J. Chem. Phys.* **2006**, *125*, 074106.

(49) Johnson, E. R. In *Non-covalent Interactions in Quantum Chemistry and Physics*; Otero-de-la-Roza, A., DiLabio, G. A., Eds.; Elsevier, 2017; Chapter 5, pp 169–194.

(50) Johnson, E. R.; Otero-de-la-Roza, A.; Dale, S. G.; DiLabio, G. A. Efficient basis sets for non-covalent interactions in density-functional theory. *J. Chem. Phys.* **2013**, *139*, 214109.

(51) Otero-de-la Roza, A.; Johnson, E. R.; Luaña, V. Critic2: a program for real-space analysis of quantum chemical interactions in solids. *Comput. Phys. Commun.* **2014**, *185*, 1007–1018.

(52) Johnson, E.; Keinan, S.; Mori-Sánchez, P.; Contreras-García, J.; Cohen, A.; Yang, W. Revealing Noncovalent Interactions. *J. Am. Chem. Soc.* **2010**, *132*, 6498–6506.

(53) Contreras-García, J.; Johnson, E. R.; Keinan, S.; Chaudret, R.; Piquemal, J. P.;

Beratan, D. N.; Yang, W. NCIPLOT: A Program for Plotting Noncovalent Interaction Regions. *J. Chem. Theory Comput.* **2011**, *7*, 625.

(54) Pyykkö, P.; Atsumi, M. Molecular Single-Bond Covalent Radii for Elements 1–118. *Chem. Eur. J. 15*, 186–197.

(55) Schmidbaur, H.; Schier, A. π-Complexation of Post-Transition Metals by Neutral Aromatic Hydrocarbons: The Road from Observations in the 19th Century to New Aspects of Supramolecular Chemistry. *Organometallics* **2008**, *27*, 2361–2395.

TOC Graphic

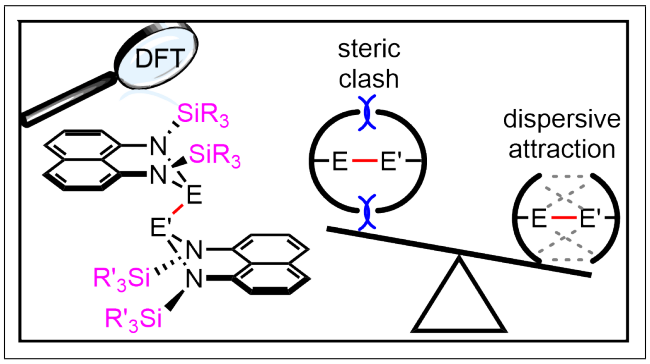
DFT
SiR3
SiR3
N
N
E
E'
N
N
R'3Si
R'3Si
steric
clash
E
E'
dispersive
attraction
E
E'